



Integration of allometric equations in the water cloud model towards an improved retrieval of forest stem volume with L-band SAR data in Sweden

Maurizio Santoro ^{a,*}, Oliver Cartus ^a, Johan E.S. Fransson ^b

^a GAMMA Remote Sensing, 3073 Gümpligen, Switzerland

^b Department of Forest Resource Management, Swedish University of Agricultural Sciences, 901 83 Umeå, Sweden



ARTICLE INFO

Keywords:

SAR
Backscatter
Forest
Stem volume
Sweden
Biomass
ALOS PALSAR
LiDAR
ICESat GLAS
Allometry

ABSTRACT

Much attention is paid to the estimation of forest biomass-related variables (stem volume and above-ground biomass) with synthetic aperture radar (SAR) backscatter images because of the increasing number of sensors in space providing global and repeated coverage and the sensitivity of the backscattered intensity to forest properties. One of the most popular models used to estimate a biomass-related variable from SAR backscatter observations is the Water Cloud Model (WCM) because of its simplicity allowing for a straightforward retrieval. Nonetheless, a common feature of these estimates is the tendency to over- or underestimate specific ranges due to simplifying assumptions in the model. In this study, the WCM has been revisited by exploring pathways for a physically-based, Light Detection and Ranging (LiDAR)-aided, model parameterization at larger scale with the overall aim to reduce systematic retrieval errors associated with empirical assumptions in the model. The study was undertaken in Sweden where repeated observations of backscatter by the Advanced Land Observing Satellite (ALOS) Phased Array-type L-band Synthetic Aperture Radar (PALSAR) were available. The integration was prototyped in Sweden thanks to detailed allometries relating forest variables in the WCM. These were derived from spatially dense estimates of canopy density and vegetation height from observations by the Ice, Cloud and land Elevation Satellite (ICESat) Geoscience Laser Altimeter System (GLAS) and measurements of height and stem volume from the Swedish National Forest Inventory (NFI). The SAR backscatter predicted by the revisited WCM was in strong agreement with the observations. When evaluated against stem volumes estimated from the NFI data, the SAR-based stem volumes presented strong dispersion at the pixel level. Average stem volume at the level of five or more pixels, i.e., for an area larger than 0.3 ha, were instead unbiased and similar to the average values obtained from the NFI data (relative root mean square error: 21.4%, estimation bias: 0.9 m³/ha and coefficient of determination: 0.67). This study demonstrates that the integration of allometries in the WCM effectively reduces estimation errors. The method here prototyped in Sweden qualifies to provide large-scale estimates of biomass-related variables using multiple observations of L-band backscatter with potential application worldwide.

1. Introduction

Forests represent the major pool of biomass on land (Bar-On et al., 2018), having substantial impact on climate because of their capacity to remove carbon from the atmosphere through photosynthesis and to release carbon through disturbances (Ciais et al., 2014). Estimation of forest biomass with spaceborne remote sensing data is a major topic of investigation since on ground measurements are able to achieve large coverage only with major surveys lasting multiple years, such as those undertaken by National Forest Inventories (Alekseev et al., 2019; Gillis

et al. 2005; Tomppo et al., 2010). The increasing amount of synthetic aperture radar (SAR) images coincides with an increasing number of investigations that focus on the estimation of forest biomass (Koch, 2010; Lu et al., 2016; Santoro and Cartus, 2018). Although the intensity of the backscattered signal shows less sensitivity to biomass-related variables than the observables from SAR interferometry and polarimetric interferometry, it is a widely used predictor because of its simplicity and the global availability (Santoro and Cartus, 2018).

To estimate a forest variable related to its biomass, i.e., above-ground biomass or stem volume, images of the SAR backscatter

* Corresponding author.

E-mail addresses: santoro@gamma-rs.ch (M. Santoro), cartus@gamma-rs.ch (O. Cartus), Johan.Fransson@slu.se (J.E.S. Fransson).

acquired at L-band (23 cm wavelength) are favored over shorter wavelength data because of the stronger penetration of the radar signal into the forest canopy, thus being sensitive to tree elements contributing the most to the biomass. Among microwave frequencies used in space, L-band SAR observations of the backscattered intensity yield estimates with higher accuracy compared to C- or X-band (Cartus and Wegmüller, 2019; Kurvonen et al., 1999; Ranson et al., 1997; Santoro et al., 2019). The availability of multiple observations is of additional benefit to reduce the effect on the backscatter signal of factors not related to the vegetation, which are acquisition-specific (Pulliainen et al., 1999; Santoro et al., 2006). During the Advanced Land Observing Satellite (ALOS) mission (2006–2011), the Phased Array type L-band Synthetic Aperture Radar (PALSAR) sensor was operated to acquire image datasets in periods when the thematic information content was maximized to support forest-related investigations (Rosenqvist et al., 2014). Over boreal forests for example, acquisition of multiple dual-polarized images was scheduled between spring and autumn when the radiometric contrast between sparsely vegetated and dense forest areas was largest compared to frozen conditions (Antropov et al., 2013; Cartus et al., 2012b; Santoro et al., 2006, 2015). The accuracy of the biomass estimated from ALOS PALSAR and its successor ALOS-2 PALSAR-2 benefited from such observation strategy. The root mean square error (RMSE) relative to the mean value from the reference data was around 25–45% at the hectare level (Antropov et al., 2013; Cartus and Wegmüller, 2019; Santoro et al., 2015, 2019). Overall, the estimates obtained in such studies were almost unbiased, thus extending the range of reliably estimated biomass beyond the level at which a single observation of the L-band backscatter becomes almost insensitive to biomass. The error was mostly explained as a consequence of the variance of the estimates due to the weak sensitivity of the L-band backscatter to biomass in high biomass forest.

The first retrieval models that used L-band SAR backscatter data as predictors were tailored to the research site and were parameterized to best fit remote sensing observations and corresponding biomass measured on the ground (Dobson et al., 1992; Harrell et al., 1995; Imhoff, 1995; Kasischke et al., 1994; Luckman et al., 1997; Ranson et al., 1995). With the availability of wall-to-wall coverages by a single sensor, the focus shifted from locally best performing models to large-scale high-performance models (Bouvet et al., 2018; Carreiras et al., 2013; Mitchard et al., 2009; Ryan et al., 2012; Sarker et al., 2012; Thapa et al., 2015; Yu and Saatchi, 2016). Retrieval models were developed to perform equally well across landscapes of a country or biome at the expenses of the retrieval error, which was tolerated to be higher than the error obtained with a more sophisticated approach.

The availability of spatially consistent datasets of L-band imagery acquired in a relatively short time period by ALOS PALSAR favored the development of approaches aimed at mapping the biomass at country scale (Carreiras et al., 2012; Cartus et al., 2012b, 2014; Mermoz et al., 2014). Non-parametric methods have the advantage that the map producer concentrates on optimizing the performance of the retrieval (Carreiras et al., 2012; Cartus et al., 2012a). The usually high accuracy reported in such studies explains the increasing attention to machine learning for mapping biomass. The main disadvantage of non-parametric methods is that they cannot be reproduced by an equation to allow an exploration of potential flaws in the relationship established by the algorithm between the backscatter observations and the biomass variable of interest. Parametric models instead try to describe such relationship by interpreting the SAR backscatter as a combination of individual scattering mechanisms (Antropov et al., 2013; Bouvet et al., 2018; Cartus et al., 2012b; Michelakis et al., 2015). The model parameters can be tuned to fit such relationship; nonetheless, parametric models entail a small number of parameters in order to ensure stability of the estimation. This requirement implies a number of approximations and generalizations, which ultimately may reduce the accuracy of the retrieval.

The Water Cloud Model (WCM) is one of the most used parametric models. It explains the backscattered signal from the vegetation in terms

of scattering mechanisms from the canopy and the ground underneath (Attema and Ulaby, 1978). Each mechanism is expressed as a simple function of a small number of parameters and variables related to either structural or biophysical properties of the vegetation and the ground. Because of its simplicity, the WCM has been tailored to express the SAR backscatter as a function of a forest biomass variable with the scope of supporting mapping of large areas (Bouvet et al., 2018; Cartus et al., 2012b; Mermoz et al., 2014). In our understanding, such simplifications made the WCM rather empirical and were the reason for some of the systematic estimation error reported in the validation of the estimates.

Differently than empirical WCM models where the SAR backscatter and the biomass variable of interest are related by regression coefficients, the parameters of semi-empirical expressions (Askne et al., 1997; Pulliainen et al., 1994; Fransson and Israelsson, 1999) are explained by forest structural and dielectric properties governing the backscatter from a forest. The performance of the semi-empirical WCM to represent the relationship between SAR backscatter and a biomass variable has been demonstrated across a wide range of spaceborne SAR observations (Fransson and Israelsson, 1999; Kurvonen et al., 1999; Pulliainen et al., 1999; Santoro et al., 2006; Santoro et al., 2019). Nonetheless, the assumptions that simplify the relationship between forest variables in order to make the WCM invertible implied an insufficient description of the relationship between the SAR backscatter and the forest biomass variable of interest in specific ranges of the latter.

To overcome such limitations, we set objective of our study to revisit the original WCM proposed in Askne et al. (1997) and integrate two sets of allometric models describing the functional dependencies between the forest variables of the WCM (canopy density and height) and forest stem volume to allow for a retrieval of the latter. By integrating allometric functions that replace empirical coefficients, we aimed at i) reducing systematic retrieval errors associated with an insufficient characterization of the relationship between forest structure as seen by a radar and stem volume in the model, and ii) exploring pathways for a physically-based model parameterization at larger scale. The forest biomass variable of interest in this study was chosen to be the stem volume of the forest, i.e., the volume of the tree trunks over bark per unit area (expressed in m³/ha). Stem volume, also known as growing stock volume, is used by countries within the boreal and temperate zone to quantify forest resources and is the prime variable to derive above-ground biomass and carbon stocks (Jenkins et al., 2003; Zianis and Mencuccini, 2004). Development and assessment of the integrated WCM was undertaken across Sweden where a multi-temporal dataset of ALOS PALSAR backscatter observations was available and detailed allometric models between forest variables could be established thanks to spatially dense observations from spaceborne LiDAR and the Swedish National Forest Inventory. Because the overall objective of our study was geared towards an improvement of a well-established framework to estimate stem volume from SAR backscatter, the spaceborne LiDAR observations served the purpose of supporting the derivation of the allometries. A benchmarking exercise with a more common use of LiDAR-derived biomass jointly with SAR observations to obtain spatially explicit estimates of biomass in a multi-variate regression scheme (Sun et al., 2011; Mitchard et al., 2012; Yu and Saatchi, 2016) was beyond the scope of this work but is seen as a theme for future investigations.

2. Study site and reference data

Sweden covers 450,295 km² with 55% of the country being forested. Forests are mostly managed for timber production. Boreal and hemiboreal coniferous species (Norway spruce and Scots pine) are dominant. Birch is the main deciduous tree species.

For the development of the retrieval model, we used waveform data acquired by the Geoscience Laser Altimeter System (GLAS) instrument onboard the Ice, Cloud and land Elevation Satellite (ICESat) (Section 2.1) and forest field inventory measurements by the Swedish National Forest Inventory (NFI) (Section 2.2). The latter dataset was also used to

assess the stem volume estimated with the proposed retrieval method.

For the assessment of the model performance, we considered a map dataset of forest stem volume produced by the Swedish University of Agricultural Sciences in co-operation with the Swedish Forest Agency. The dataset was based on a nation-wide coverage of airborne laser scanning (ALS) waveforms collected by the Swedish National Land Survey (Lantmäteriet) (Nilsson et al., 2017) (Section 2.3). The reason for using this spatially explicit dataset of stem volumes was the much larger number of samples compared to the NFI dataset to allow for local assessments of the retrieval model.

2.1. ICESat GLAS estimates of canopy density and height

Between 2003 and 2009, ICESat GLAS measured energy returned from the Earth surface in ca. 65 m large footprints collected every 170 m along track. The sampling was sparser across track because of the large distance between adjacent orbits (60 km at the Equator) (Los et al., 2012). The returned signal from a forest was affected by density, shape and reflectivity of leaves, needles and branches in each layer of the forest canopy. For this study, we used waveform data over land only described in the form of the parameters of a multi-Gaussian model fitted to the raw waveforms (GLA14 product provided by the National Snow & Ice Data Centre, <https://nsidc.org/data/icesat/data.html>). For each footprint, we estimated canopy density and canopy height from the waveform parameters.

Canopy density (CD) was defined as the ratio of energy received from the canopy (returns above the ground peak) to the total energy received (Hilbert and Schmullius, 2012). To account for differences in the reflectivity of canopy and forest floor, canopy density estimates derived from GLAS (CD_{GLAS}) were corrected according to:

$$CD = \frac{CD_{GLAS}}{CD_{GLAS} + 0.5(1 - CD_{GLAS})} \quad (1)$$

assuming that forest floor and canopy reflectivity differ by a factor 2. Canopy height was defined as the relative height of the first return with respect to the last return ($RH100$) (Los et al., 2012; Simard et al., 2011). A set of filters was defined to discard footprints affected by topography and various noise sources in the waveforms (Simard et al., 2011) resulting in a global dataset of CD and $RH100$ measurements for approximately 26.5 million footprints over vegetated terrain of which 38,358 were located in Sweden.

2.2. Swedish national forest inventory

The statistical design of the Swedish NFI is based on systematic cluster sampling, using forest field inventory plots arranged in rectangular clusters, referred to as tracts. Each tract has a side length between 300 m and 1800 m, and consists of either 4–8 permanent or 8–12 temporary inventory plots regularly spaced along the perimeter of the tract. The spatial separation in the North-South and East-West direction between adjacent tracts increases from 10 km in South Sweden to 20 km in North Sweden. Each of the approximately 30,000 permanent plots has a radius of 10 m, corresponding to an area of 0.03 ha, and is revisited every five years, i.e. 1/5 of the permanent clusters are measured every year. Each year, in addition, 10,000 temporary plots are established to increase the sampling achieved with the permanent plots. A temporary plot has a radius of 7 m, corresponding to 0.015 ha, and is measured once. The position of the inventory plots is determined from differential GPS with a nominal accuracy of about 5 m. The scope of the inventory plots is to derive official statistics of forest properties at the level of administrative or ecological units. As a consequence, individual measurements are not optimized to calibrate remote sensing models or to evaluate retrieval models because of the different sampling and the smaller area compared to remote sensing observations.

The NFI dataset of stem volumes used in this study consisted of

measurements at permanent plots surveyed in 2010 and at temporary plots surveyed between 2009 and 2011, resulting in a total of 6215 records. A dataset of NFI plot measurements spanning three years of measurements allowed for a rather homogeneous coverage of the whole country (Fig. 1d). Stem volume ranged between 0 m³/ha and 1051 m³/ha although for 95% of the plots, it was less than 400 m³/ha, roughly corresponding to an above-ground biomass of 200 tons/ha (Fig. 1a). After grouping plots according to the predefined 30 km × 30 km grid (see Section 3), the average stem volume and the number of inventory plots were computed per tile (Fig. 1c and d). The average stem volume was between 7 m³/ha and 346 m³/ha (Fig. 1b) based on between 1 and 54 inventory plots per tile from in total 444 tiles. Stem volume increased with decreasing latitude, corresponding to the transition from boreal to hemiboreal forests (Fig. 1c). For North and Central Sweden, stem volume was higher along the East coast compared to the inland (Fig. 1c).

2.3. ALS-based dataset of stem volume

ALS data collected between 2009 and 2015 over Sweden were used to generate a set of maps of forest variables with a pixel size of 12.5 m × 12.5 m (Nilsson et al., 2017). NFI data collected between 2009 and 2013 were used to train linear regression models relating the forest variables to ALS metrics. The accuracy of the stem volume estimates at the level of forest stands was in the range of 17.2–22.0% (relative RMSE). The database of ALS-based maps is available from the Swedish Forest Agency's homepage (<http://www.skogsstyrelsen.se/skogligagrunddata>, last accessed on 14 September 2020). As the objective of this study was to demonstrate a new framework for estimating stem volume from SAR data, we consider the ALS-based dataset purely to assess the performance of the retrieval model. An inter-comparison of AGB or stem volume maps derived from different sensors, including this one, was beyond the scope of this paper.

3. SAR dataset

The SAR dataset consisted of ALOS PALSAR images acquired in the Fine Beam Dual (FBD) mode at HH- and HV-polarization over Sweden. The best one-year coverage was obtained in 2010, when 99% of the country area was imaged during four cycles in FBD mode scheduled between May and October. The gap was filled with images acquired during summer 2008, these being the data closest in time to the 2010 dataset that could fill the gap.

The 2010 dataset was generated by the Japan Aerospace Exploration Agency (JAXA) Earth Observation Research Centre (EORC) and consisted of 104 image strips of detected SAR backscatter. All images were acquired along an ascending orbit, i.e. at approximately 10:30 p.m. local time. The data were provided in the radar geometry and had been spatially averaged by JAXA from Single Look Complex (SLC) format to backscatter images with a pixel size of approximately 25 m in each direction. The images acquired in 2008 were obtained from JAXA as individual image frames in SLC format. Frames belonging to the same orbital track were concatenated to form image strips. Detected SAR images of the backscattered intensity with the same pixel size as the 2010 dataset were obtained by multi-looking the concatenated SLCs with factors 2 and 8 in range and azimuth, respectively.

Each image strip was calibrated using factors provided by JAXA (−83 dB) (Shimada et al., 2009) and terrain geocoded using the national DEM of Sweden with a pixel size of 50 m (Lantmäteriet, 2010). To preserve the original pixel size of the image strips, the DEM was oversampled to 25 m in northing and easting with bilinear interpolation; we assumed that this geometric transformation did not alter the geometric and thematic accuracy of the data product (Lantmäteriet, 2019). The geocoding procedure was based on a look-up table relating the pixel coordinates of the radar and the map geometry (Wegmüller, 1999). To cope with inaccuracies of the image metadata that would cause imperfections in the transformation described by the look-up table, this was

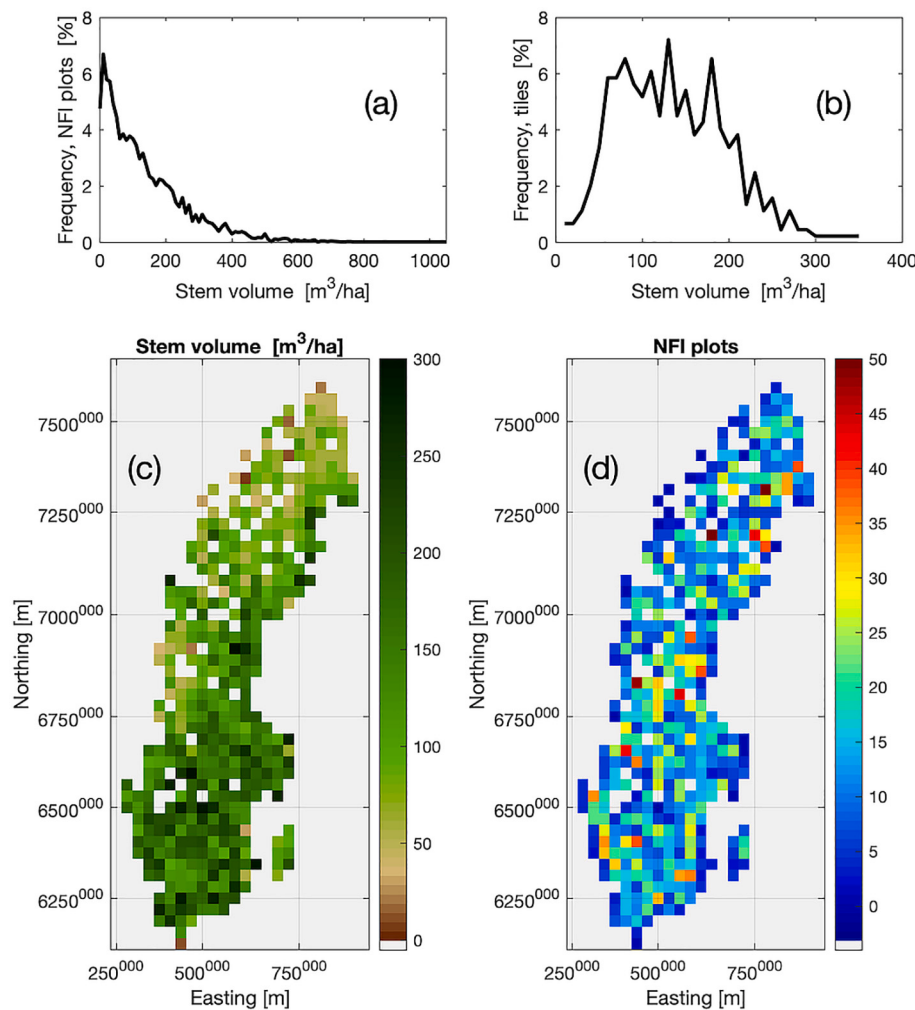


Fig. 1. Histogram of NFI stem volumes based on 6215 inventory plots measured between 2009 and 2011 in Sweden (a). Histogram of tile-based average stem volume from the Swedish NFI dataset (b). Map of average NFI-based stem volumes per tile (c) and number of inventory plots per tile (d).

refined by estimating co-registration offsets in range and azimuth between the image strip in radar geometry and an image assumed to be in the reference map geometry and transformed to the radar geometry with the look-up table. The reference image was typically a radar image simulated from the DEM with parameters of the actual SAR image unless the image strip covered largely flat terrain in which case a mosaic of Landsat images put in the geometry of the DEM was used. Offsets were estimated with a cross-correlation algorithm in windows of 256 by 256 pixels equally distributed all over the SAR image (Wegmüller et al., 2002) and then modeled with a second order polynomial as a function of range and azimuth (i.e., x and y Cartesian coordinates). After the refinement of the look-up table with the offset models, the co-registration accuracy was on average 0.1 times the size of the pixel, i.e., 2.5 m, and never larger than 0.3 times the pixel size, i.e., 8 m. Each geocoded SAR image strip was finally normalized for slope-induced effects on the backscatter (Ulander, 1996).

Each geocoded image strip was tiled into a pre-defined grid, each tile being 30 km × 30 km large. The size of a tile was set so that the computing resources could be optimized when estimating stem volume. The size of a tile was also a trade-off between having a sufficiently large number of samples in each tile to obtain a reliable estimate of the average stem volume from the reference dataset (Section 2.2) and capturing the spatial patterns of stem volume across the country.

No additional speckle filter was applied since a visual analysis of the geocoded images revealed clear fine-scale textural features that would

have been lost otherwise. Thanks to the availability of repeated image acquisitions in a single year and partial overlap of swaths for adjacent orbital tracks, each pixel was characterized by a multi-temporal dataset of SAR backscatter observations. On average, 8 observations per pixel were available consisting of 4 co-polarized and 4 cross-polarized measurements (Fig. 2). The dataset was denser, with up to 24 observations, in the southernmost part of Sweden (Fig. 2). Poorer coverage (2 or 4

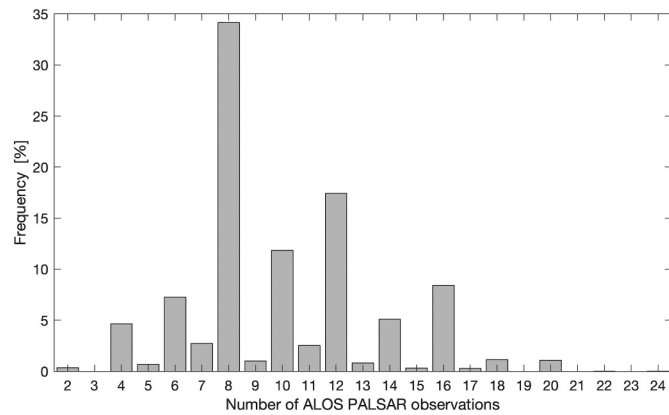


Fig. 2. Histogram of the number of ALOS PALSAR observations per pixel over Sweden.

observations) corresponded to the area that had to be gap-filled with images of 2008.

4. Methods

4.1. Allometries

In this study, allometries refer to the functional relationship between forest variables. In specific, we were interested in characterizing the dependency of the two predictors of the WCM, namely canopy density and forest height, upon stem volume (Section 4.2). The objective was to obtain an explicit and physically-based relationship of the SAR backscatter to stem volume and allow for the direct estimation of stem volume from a measurement of the SAR backscatter.

To parameterize the relationship between canopy density and height, we could not rely on measurements from a forest inventories because the former is not measured. The allometry was instead based on ICESat GLAS metrics of canopy density (CD) and canopy height (h). An analysis of functions fitted to the observations of GLAS-based canopy density and height revealed that the rise-to-max function in Eq. (2) was the most robust. In this analysis, it was assumed that the canopy height is represented by the RH100 metric and h is equal to the forest height.

$$CD = 1 - e^{-qh} \quad (2)$$

The dependence of forest height upon stem volume was described by the power-law function in Eq. (3) expressing forest height, h , as a function of stem volume, V . Eq. (3) was demonstrated using forest field inventory measurements at several sites (Askne et al., 1997; Askne and Santoro, 2012; Santoro et al., 2002).

$$h = (aV)^b \quad (3)$$

This allometry was used in previous studies modeling the interferometric response of forests at small test sites with the aim of replacing the height variable in the Interferometric Water Cloud Model with stem volume (Askne et al., 1997; Santoro et al., 2002; Askne et al., 2013; Askne and Santoro, 2015).

4.2. Forest backscatter model

The Water Cloud Model with gaps (Askne et al., 1997) in Eq. (4) is based on radiative transfer theory according to which the incoming wave is transmitted through and scattered by a cloud of droplet representing the volume formed by needles, twigs, branches and trunks. The WCM expresses the total forest backscatter as the incoherent sum of direct scattering from the ground through gaps in the canopy, ground scattering attenuated by the canopy and direct scattering from the vegetation. Multiple scattering components (e.g., trunk-ground, ground-trunk and multiple reflections) are neglected. Previous studies indicated that this is a reasonable assumption for short wavelength radar data and boreal forests (Pulliainen et al., 1999; Santoro et al., 2015, 2006).

$$\sigma_{for}^0 = (1 - \eta)\sigma_{gr}^0 + \eta\sigma_{gr}^0 T_{tree} + \eta\sigma_{veg}^0 (1 - T_{tree}) \quad (4)$$

In Eq. (4), η represents the area-fill factor, i.e., the fraction of the area covered by vegetation. The parameters σ_{gr}^0 and σ_{veg}^0 represent the backscattering coefficient of the ground and vegetation layer, respectively. T_{tree} represents the two-way tree transmissivity.

The two-way tree transmissivity is expressed as

$$T_{tree} = e^{-ah} \quad (5)$$

where α represents the two-way attenuation per meter through the tree canopy and h is the depth of the attenuating layer, which is assumed to correspond to the forest height.

Eq. (4) can be rewritten to highlight the contribution from the forest floor and the contribution from the canopy

$$\sigma_{for}^0 = [1 - \eta(1 - e^{-ah})]\sigma_{gr}^0 + \eta(1 - e^{-ah})\sigma_{veg}^0 \quad (6)$$

or likewise

$$\sigma_{for}^0 = \sigma_{gr}^0 T_{for} + \sigma_{veg}^0 (1 - T_{for}) \quad (7)$$

where the two-way forest transmissivity, T_{for} , is expressed as a function of two forest structural parameters, i.e., forest height and canopy density, and a parameter related to the capability of microwaves to penetrate through the vegetation, α .

$$T_{for} = 1 - \eta(1 - e^{-ah}) \quad (8)$$

For retrieval purposes, the backscatter should be expressed as a function of a forest variable related to the forest biomass, i.e., the forest transmissivity in Eq. (8) needs to be expressed in terms of above-ground biomass or stem volume. In previous studies, we used the expression for the WCM relating the SAR backscatter to stem volume, V (Fransson and Israelsson, 1999).

$$\sigma_{for}^0 = \sigma_{gr}^0 e^{-\beta V} + \sigma_{veg}^0 (1 - e^{-\beta V}) \quad (9)$$

In Eq. (9), β is an empirically defined coefficient expressed in ha/m^3 . Eq. (9) can in principle be derived from Eq. (6) assuming the forest to be a homogeneous volume, with attenuation parameterized in terms of number of scattering elements, thickness of the volume (i.e., vegetation height), attenuation per meter and look direction. In addition, a linear relationship between height and stem volume is assumed.

The WCM with gaps in Eq. (6) and the WCM expressing the total backscatter as a function of stem volume as in Eq. (9) become equivalent when:

$$e^{-\beta V} = 1 - \eta(1 - e^{-ah}) \quad (10)$$

In Askne and Santoro (2015), it was attempted to relate the area-fill factor to stem volume by means of the vegetation ratio, a metric derived from laser scanning data. In that study, the model was tailored to fit to the observations from the small test site under investigation. However, the equivalence of the forest transmissivity definitions postulated in Eq. (10) might be incorrect in particular in the low and medium stem volume range because the function expressing height upon stem volume is non-linear. Not accounting for the non-linearity implies a systematic error affecting stem volume estimated from the WCM.

Assuming that the area-fill factor can be approximated with canopy density, Eq. (8) can be rewritten to capture the dependency of the forest transmissivity on stem volume, V , by means of the allometries proposed in Section 4.1.

$$T_{for} = f(\eta, h, \alpha) = f(\eta(h(V)), h(V), \alpha) \quad (11)$$

By replacing T_{for} in Eq. (7) with Eq. (11) accounting for the allometries, the total forest backscatter (observable, σ_{for}^0) is expressed in Eq. (12) as a function of stem volume through

- the backscatter parameters of the ground and the vegetation (σ_{gr}^0 and σ_{veg}^0 , respectively) and the two-way tree transmissivity, α , which are unknown;
- the parameters of the allometric relationships in Eqs. (2), (3) (q , a and b).

$$\sigma_{for}^0 = \sigma_{gr}^0 \left(e^{-q(aV)^b} + e^{-a(aV)^b} - e^{-(q+a)(aV)^b} \right) + \sigma_{veg}^0 \left(1 - e^{-q(aV)^b} - e^{-a(aV)^b} + e^{-(q+a)(aV)^b} \right) \quad (12)$$

4.3. Estimation of the model parameters

The estimation of the model parameters σ_{gr}^0 and σ_{veg}^0 was undertaken separately for each image and each tile to account for spatial and temporal variability of the SAR backscatter. Since σ_{gr}^0 and σ_{veg}^0

represent the backscattered intensity for an unvegetated natural surface and for a completely opaque canopy, respectively, a pragmatic approach to estimate them is to select the backscatter measurements in correspondence of low and high canopy cover and set each estimate equal to an average value of the selected measurements. The approach was originally developed for the training of the WCM using hyper-temporal C-band SAR backscatter observations (Santoro et al., 2011) and is used here to overcome the issue of uncertain model predictions when obtained from a limited number of reference observations in a training dataset such as when a sparse network of measurements are available. Here, we summarize the main aspects of the approach presented in Santoro et al. (2011), providing additional details where the implementation in this study differed compared to the original version of the approach.

This self-calibrating approach to estimate σ_{gr}^0 and σ_{veg}^0 requires an auxiliary dataset of canopy density, such as the Moderate Resolution Imaging Spectroradiometer (MODIS) Vegetation Continuous Fields (VCF) of vegetation cover (Hansen et al., 2003). The advantage of the MODIS VCF dataset over other spatially explicit datasets of canopy cover (Hansen et al., 2013; Sexton et al., 2013) is the availability of an annual basis and the coarser spatial resolution, which speeds up the computation of the model parameters. For model training, the percent tree cover layer of the MODIS VCF product is used as a mask in order to select backscatter measurements belonging to a certain category of canopy densities.

In this study, we set the estimate of the model parameter σ_{gr}^0 equal to the median value of the SAR backscatter in correspondence of MODIS VCF pixels below a certain threshold on canopy cover. The threshold corresponded to the smallest canopy density between 15% and 30% satisfying the requirement that at least 0.3% of the pixels in the tile had been selected.

The median of the backscatter histogram for pixels characterized by a dense forest canopy, here referred to as σ_{df}^0 , does not correspond to an estimate of σ_{veg}^0 because the backscatter of dense forests contains a contribution from the ground through the gaps in the canopy. An estimate of σ_{veg}^0 is obtained from σ_{df}^0 by compensating for the residual ground contribution, $\sigma_{gr}^0 T_{df}$. This step is explained when inverting Eq. (7) to express the backscattering coefficient σ_{veg}^0 as a function of the other model parameters.

$$\sigma_{veg}^0 = \frac{\sigma_{df}^0 - \sigma_{gr}^0 T_{df}}{1 - T_{df}} \quad (13)$$

An estimate of the coefficient T_{df} was set equal to the median value of the SAR backscatter for MODIS VCF pixels above a given threshold on canopy cover. Here, the threshold was 85% of the maximum canopy density in the tile of interest. The estimate of the two-way forest transmissivity of dense forests (T_{df}) was obtained in Eq. (14). This was derived from Eq. (8) and required values representative for the canopy cover of dense forests, η_{df} , and the forest height for dense forests, h_{df} . The parameters η_{df} and h_{df} were defined as the average of the canopy density and canopy height values for the subset of LiDAR footprints with canopy density larger than the predefined threshold in a tile, respectively. The two-way tree attenuation, α , depended on the structural and dielectric properties of a tree. In literature, we find a relatively small number of studies targeting the quantification of tree attenuation; for boreal forests, a generic consensus appeared to consider realistic α around 0.5 dB/m at L-band (Santoro et al., 2006). This aspect was further investigated in Section 5.3.

$$T_{df} = 1 - \eta_{df} (1 - e^{-ah_{df}}) \quad (14)$$

Since the estimation of the model parameters was undertaken for each tile, an insufficient number of pixels selected to estimate σ_{gr}^0 (e.g., high density forest landscape) or σ_{df}^0 (e.g., very sparse forest cover) within the tile implied a missing value. To overcome gaps in the field of estimates of the model parameters for a given image, an estimate was

still obtained by interpolating over valid values in neighboring tiles.

4.4. Stem volume retrieval

Once all model parameters are known and the allometries have been set, the model in Eq. (6) expressed as a function of stem volume was inverted to obtain an estimate of stem volume for an observation of the SAR backscatter. The inversion was implemented in a numerical approach and identified the stem volume for which the difference between observed backscatter and modeled backscatter from Eq. (6) was smallest. The inversion rules for measurements falling outside of the range of backscatter values predicted by Eq. (6) associated either the value 0 for measurements below the minimum modeled backscatter or a maximum retrievable stem volume (Santoro et al., 2011) for measurements above the maximum modeled backscatter. The maximum retrievable stem volume was defined on a tile by tile basis as the 90th percentile of the NFI plots, further increased by 50 m³/ha (Santoro et al., 2011).

Since the ALOS PALSAR dataset allowed for multiple estimates of stem volume, a final estimate of the stem volume, V_{mt} , was obtained with a weighted average of the individual estimates, V_i (Kurvanen et al., 1999).

$$V_{mt} = \frac{\sum_{i=1}^N w_i V_i}{\sum_{i=1}^N w_i} \quad (15)$$

with $w_i = (\sigma_{veg,i}^0 - \sigma_{gr,i}^0)$ being defined as the difference between the estimates of the modeled backscattering coefficients for the specific image, i . The benefit of a weighted average is that the accuracy of the stem volume estimate is improved with respect to each of the individual estimates (Cartus et al., 2012b; Santoro et al., 2006).

4.5. Validation

To validate the stem volume estimates from Eq. (15), we used the dataset of NFI stem volumes. It is remarked that these were not used to train the WCM, thus, being independent from the ALOS-based estimates. A plot-to-pixel comparison, however, had little explanatory power to allow for a correct assessment of the estimates for several reasons. Inventory plots and pixels did not match in size and their values were obtained from two different survey points of view (side-ways and sensing the canopy vs. vertically and measuring the trunk). Furthermore, a plot might have covered an area included in several adjacent pixels. Finally, both plots and pixels had a geolocation uncertainty. Still, a plot-to-pixel comparison is reported for completeness to confirm the ill-posed setting of the comparisons.

To account for partial overlap between plot area and pixel area, an area-weighted average of the stem volume estimates for each pixels covered by a plot was computed. Then, to account for the geolocation uncertainty of plots and pixels, the procedure was repeated $M = 100$ times, each time shifting randomly the location of the plot and the stem volume map using uncertainty information published for the inventory plots (Section 2.2) and computed for the SAR imagery (Section 3). The M weighted averages of the stem volume estimates for a given inventory plot were finally averaged to obtain the stem volume estimate used to compare against the corresponding stem volume from the field inventory plot.

5. Results

5.1. Relating forest canopy density to forest height

Fig. 3 shows that the curve predicted by the model in Eq. (2) corresponded to the ICESat GLAS metrics, although these were

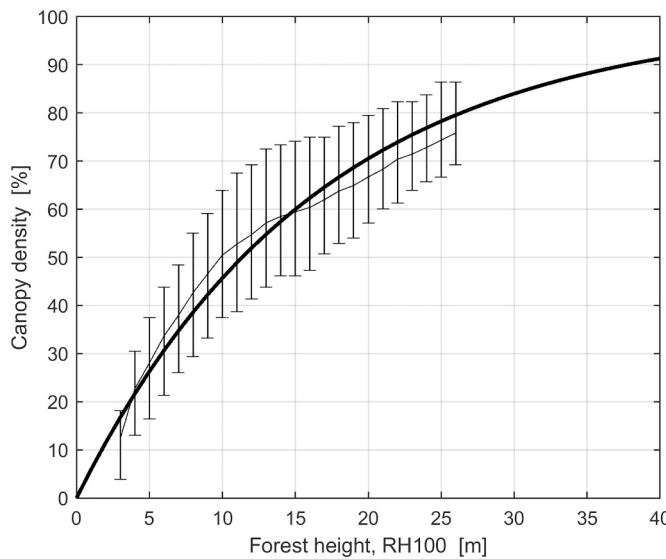


Fig. 3. Observations of ICESat GLAS canopy density and canopy height (RH100 metric) for Sweden arranged in the form of vertical bars representing the interquartile range of canopy density for a given canopy height. The thin solid segments connect the median values of the canopy density observations per canopy height interval. The solid curve represents the least squares regression of Eq. (2) to the observations ($R^2 = 0.42$). The curve was extended to cover the range 0–40 m of potential forest heights in Sweden. The estimate of the coefficient q in Eq. (2) corresponding to the solid curve is 0.0611.

characterized by strong dispersion, which explains the low coefficient of determination (R^2) of 0.42.

To understand whether the dispersion of the canopy density vs. height observations was due to the spatial patterns associated with a diversity of forest structures across the country, we stratified the observations by the $30 \text{ km} \times 30 \text{ km}$ ALOS PALSAR tiles and fitted Eq. (2) to the data in each tile. The map of the estimates of the parameter q obtained with non-linear regression (Fig. 4, left panel) shows faint spatial trends. The noisiness of the spatial distribution of the parameter's estimates was explained as a consequence of a spatially variable number of GLAS observations available in a tile (Fig. 5) as well as the moderate association between the observations of canopy density and height (median R^2 : 0.44; inter-quartile range of R^2 : 0.25–0.56).

After discarding estimates of the parameter q based on less than 60 GLAS observations because of noisy estimates (Fig. 5), filling gaps with a two-dimensional interpolator based on inpainting applied to the

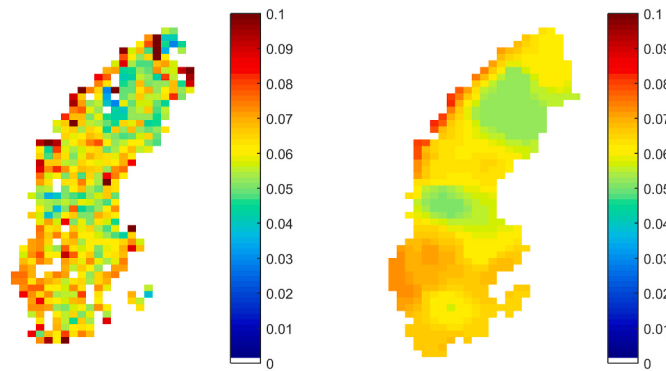


Fig. 4. Estimates of the parameter q in Eq. (2) over Sweden for each of the $30 \text{ km} \times 30 \text{ km}$ ALOS PALSAR tiles. The left panel shows the original estimates obtained from non-linear regression using the GLAS metrics of canopy density and canopy height as predictors. The right panel shows the result of post-processing after removal of noisy estimates, interpolation and 3×3 median filtering.

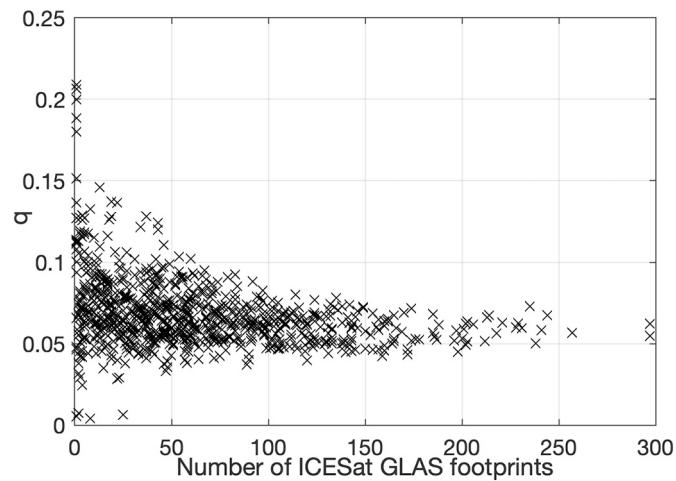


Fig. 5. Number of ICESat GLAS footprints, i.e., observations, and corresponding estimates of the parameter q in Eq. (2) for each of the $30 \text{ km} \times 30 \text{ km}$ ALOS PALSAR tiles.

remaining estimates of q and 3×3 median filtering, we obtained a clearer indication on the spatial patterns of this parameter (Fig. 4, right panel). Regions appearing in green and yellow corresponded to a somewhat sparser forest cover. On the other hand, regions appearing in red corresponded to forests with denser canopies for increasing canopy height. The largest estimates were found in the north-western part of the country, in correspondence of the border to Norway, an area characterized by moderate to strong topography. These results may be interpreted as an effect of residual topographic effects in the GLAS waveform metrics, which altered the true relationship between canopy density and canopy height.

5.2. Relating forest height to stem volume

The curve in Fig. 6 represents the fit of Eq. (3) to all measurements of forest height and stem volumes from the NFI. The relationship between

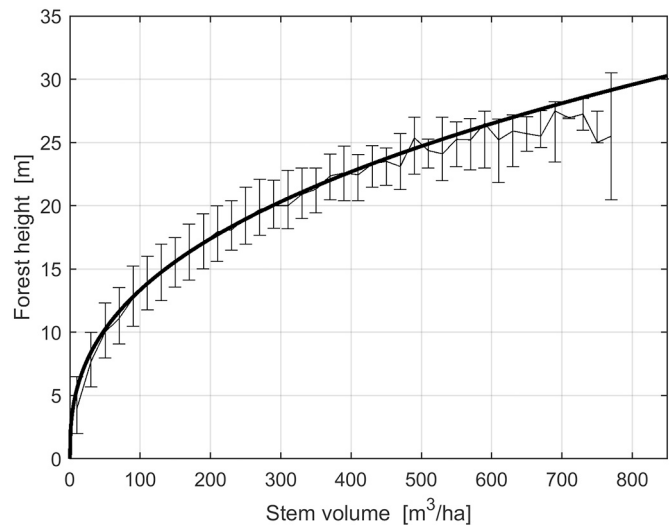


Fig. 6. Observations of forest height and stem volume from the dataset of inventory plots of the Swedish NFI and corresponding model fit from Eq. (3). The thin solid segments connect the median values of forest height observations stratified into $20 \text{ m}^3/\text{ha}$ wide intervals of stem volume. The vertical bars represent the interquartile range of forest height measurements for each interval of stem volume. The solid curve represents the non-linear regression obtained with Eq. (3) ($R^2 = 0.73$). The estimates of the parameters in Eq. (3) are $a = 8.7105$ and $b = 0.3827$.

the two forest variables was well explained by the power-law function of Eq. (3) ($R^2 = 0.73$). Similarly to the case of canopy density and canopy height, the dispersion of the measurements illustrated by the vertical bars in Fig. 6 indicated that there might have been differences in how stem volume and height are related across the country. The relationship between height and stem volume depends indeed on stocking (Santoro et al., 2007), which in turn depends on climatic and geographic patterns (macro-scale conditions) as well as forest management practices (micro-scale condition). Forests characterized by higher stem density levels present higher stem volume for a given height. Even by restricting to a smaller area with similar forest cover properties, e.g., sparse boreal forest, a spatially detailed parameterization of the height-to-volume function is impossible due to the very local forest management practices in Sweden. To illustrate the spatial variability of the height-to-volume relationship, we stratified the NFI dataset by the ALOS PALSAR tiles and estimated in each tile the parameters a and b in Eq. (3). The height predicted by the model trained at the level of individual tiles was found to differ as much as 3 m compared to the height predicted by the country-wide model (Fig. 7). The variability of the estimate of the model parameters a and b in Eq. (3), however, did not depend on the geographic location of the tile. For the retrieval, it was therefore decided to use the pair of values obtained from all the NFI data (Fig. 6), although this meant that slight systematic errors in the retrieval might have been introduced.

5.3. Estimation of tree attenuation

To verify the assumption that the estimate of the tree attenuation could be simplified to $\alpha = 0.5 \text{ dB/m}$, we simulated the forest backscatter with Eq. (7) for different α values and compared the predictions with backscatter observations. The average of the residuals between modeled and measured forest backscatter at sample pixels was used to identify the range of α values, for which the model best predicted the relationship between backscatter observations and stem volume. Since environmental conditions such as precipitation, snow wetness etc. could affect the SAR backscatter, the assessment was undertaken at the level of individual ALOS PALSAR tiles. Indeed, visual investigation of the SAR backscatter from forests appeared mostly homogeneous within tiles of

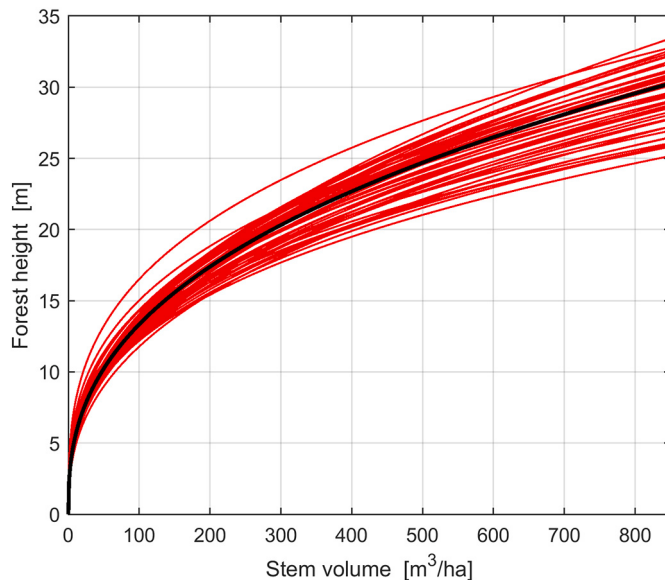


Fig. 7. The red curves represent the modeled forest height as a function of stem volume using Eq. (3) on a tile-by-tile basis. The black curve represents the modeled forest height based on data from all NFI plots illustrated in Fig. 6. (For interpretation of the references to color in this figure legend, the reader is referred to the web version of this article.)

30 km × 30 km although we did not undertake a quantitative analysis trying to relate spatial variability of the backscatter to spatial patterns of environmental conditions to confirm this.

The WCM was simulated for α varying between 0.1 dB/m and 2 dB/m in steps of 0.1 dB/m for each SAR image available for each tile. The mean value of the residuals was then computed for each α value and image in a given tile. The analysis was undertaken separately for HH- and HV-polarization.

At first, we attempted to compare modeled and observed forest backscatter at the ICESat GLAS footprints. The stem volumes necessary to simulate the backscatter were obtained at each footprint with Eqs. (2) and (3) from the corresponding measurements of CD and RH100. Because of the poor association between ALOS PALSAR backscatter measurements and stem volume at plot level, the estimates of α were often unrealistic and the uncertainty associated with the estimates was large. For this reason, we investigated the alternative use of the ALS-based dataset to represent stem volume.

Figs. 8 and 9 show examples of the average backscatter residual as function of α for a tile located in the boreal zone at a latitude of 66°N and a tile located in the hemiboreal zone at 58°N, respectively. The closest agreement between modeled and measured SAR backscatter was obtained for slightly higher α values in southern Sweden compared to northern Sweden. The estimate for α was somewhat smaller at HV-polarization compared to HH-polarization. Overall, the smallest values were estimated in the northernmost region of Lapland (0.2 dB/m and 0.1 dB/m for HH- and HV-polarization, respectively). The largest values were estimated in the Baltic Sea region of South Sweden (1 dB/m and 0.8 dB/m for HH- and HV-polarization, respectively). The value of 0.5 dB/m was obtained in Central Sweden, at about 60°N.

Although Figs. 8 and 9 show a clear minimum in the average residual as a function of α , the range of the average backscatter residuals was rather small, implying that the sensitivity of the stem volume retrieval to different α values was small. Simulations of the WCM with $\alpha = 0.5 \text{ dB/m}$ were compared with simulations of the WCM for the extreme cases of α equal to 0.1 dB/m and 1 dB/m, resulting in at most 0.3 dB difference, which corresponded to a difference of estimated stem volume of at most 20 m³/ha. The largest difference occurred for forests of medium-high stem volume where the WCM tended to flatten as stem volume increased. Taking into account the marginal effect of the value of α on the modeled backscatter and on the retrieval, it was assumed that the 0.5 dB/m level was in principle acceptable for retrieval purposes even though a more accurate characterization of the tree attenuation could be attempted in the future with more suitable data.

5.4. Verification of the two-way transmissivity term

The definition of the two-way forest transmissivity, T_{for} , in Eq. (11) was benchmarked with simulations based on Eq. (8) using as reference the canopy density and height estimates from the ICESat GLAS dataset. In addition, the forest transmissivity was estimated with the simple exponential of stem volume, i.e., $e^{\beta V}$, to verify the validity of the equivalence in Eq. (10). In this work, β was assumed to be 0.004 ha/m³, which was found to be a realistic estimate in Swedish boreal forest (Santoro et al., 2015). The forest transmissivity modeled as a function of canopy density and height reproduced the trend in the observations of forest transmissivity based on the GLAS metrics and stem volume (Fig. 10). On the contrary, the simple exponential of stem volume provided a poor fit to the observations, spanning a larger range of values and presenting a gentle slope compared to the forest transmissivity modeled as function of canopy density and height (Fig. 10).

5.5. Verification of the modeled backscatter

To assess the validity of the backscatter predicted by the WCM in Eq. (6) complemented with the allometries in Eqs. (2), (3), we compared the modeled backscatter with observations of the ALOS PALSAR backscatter

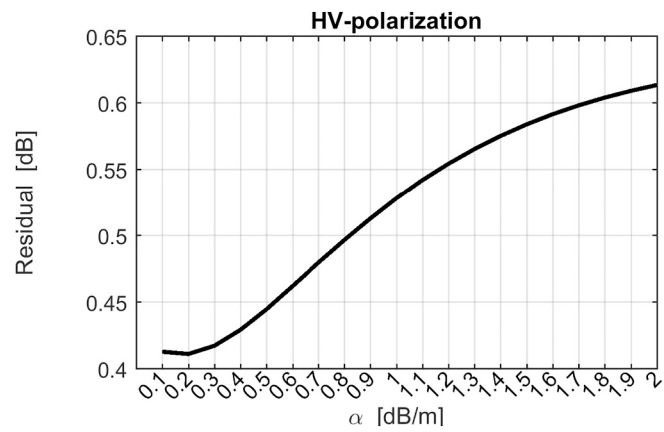
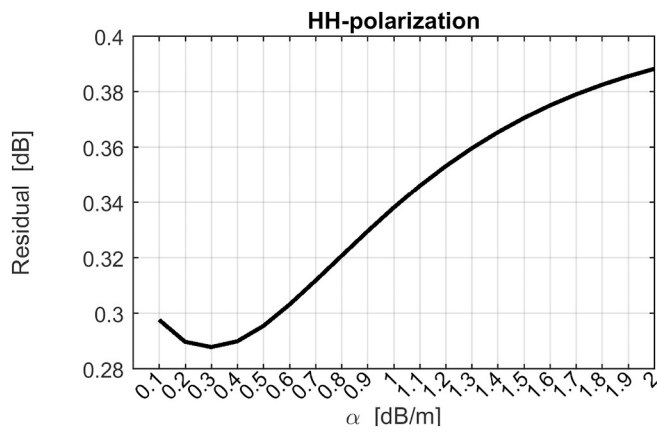


Fig. 8. Average backscatter residual as a function of α at 66°N for HH- and HV-polarization based on ALOS PALSAR multi-temporal observations of the SAR backscatter, all acquired under unfrozen conditions.

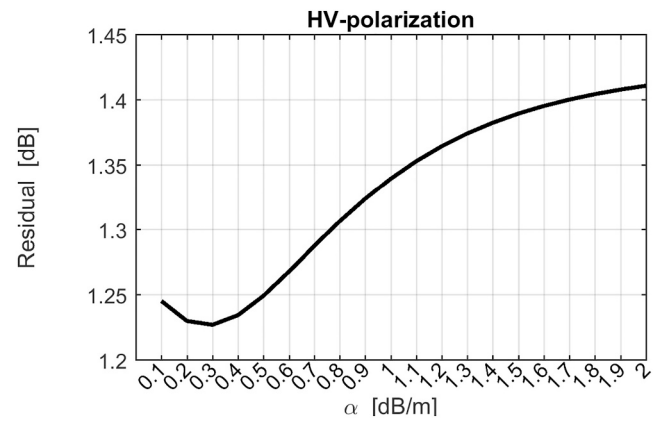
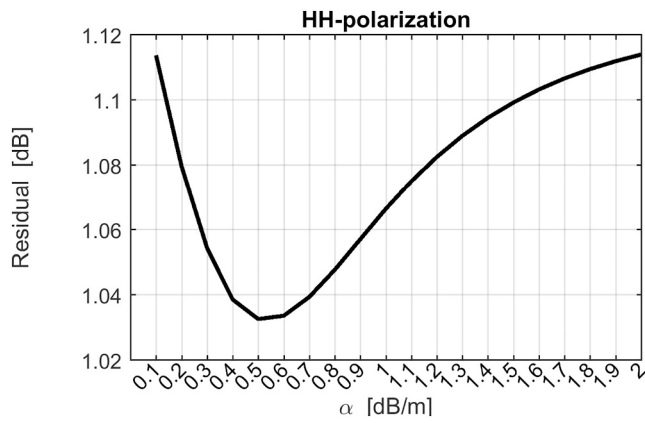


Fig. 9. Average backscatter residual as a function of α at 58°N for HH- and HV-polarization based on ALOS PALSAR multi-temporal observations of the SAR backscatter, all acquired under unfrozen conditions.

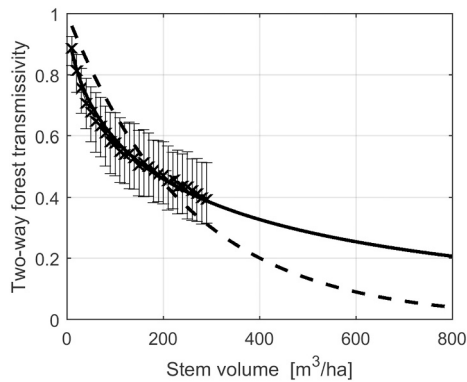


Fig. 10. Two-way forest transmissivity modeled with the two terms in Eq. (10) (dashed curve: simple exponential; solid curve: function of canopy density and height). The modeled forest transmissivity is compared to simulations obtained with Eq. (8) using observations of canopy density and height from ICESat GLAS dataset over Sweden. The simulations of the forest transmissivity were stratified by stem volume, in $10 \text{ m}^3/\text{ha}$ wide intervals, and are here represented with vertical bars, each corresponding to the interquartile range. The modeled two-way forest transmissivity is truncated at $800 \text{ m}^3/\text{ha}$ to illustrate the rate of change of the transmissivity when approaching the highest values of stem volume recorded at the field inventory plots in Sweden (Fig. 1a).

and corresponding estimates from the ALS-based dataset of stem volume. In addition, we considered the backscatter predicted by the WCM with a forest transmissivity term expressed by a simple exponential function. The assessment was undertaken on a tile-by-tile basis to allow for a characterization of the relationship between SAR backscatter and stem volume within an area where one could reasonably assume that the environmental conditions and the forest structural properties are uniform.

To verify that the definition of forest transmissivity in Eq. (8) was able to reproduce the trend of backscatter observations as a function of stem volume, we illustrate two examples of L-band backscatter observations and stem volume observations and the corresponding modeled backscatter for a tile in northern Sweden (Fig. 11) and a tile in southern Sweden (Fig. 12). The backscatter modeled as a function of canopy density and height was close to the mean trend in the observations (Figs. 11 and 12). The backscatter modeled assuming a forest transmissivity expressed as a simple exponential of stem volume did not perform equally well. With such a model, the estimation of stem volume would have resulted in a considerable overestimation in the low stem volume range, i.e., below $100 \text{ m}^3/\text{ha}$.

5.6. Stem volume retrieval

The retrieval method was used to generate a map of stem volume from the ALOS PALSAR dataset with a pixel size of 25 m (Fig. 13). For completeness, we show a comparison of the stem volume estimates and NFI measurements at the level of individual pixels and plots (Fig. 14).

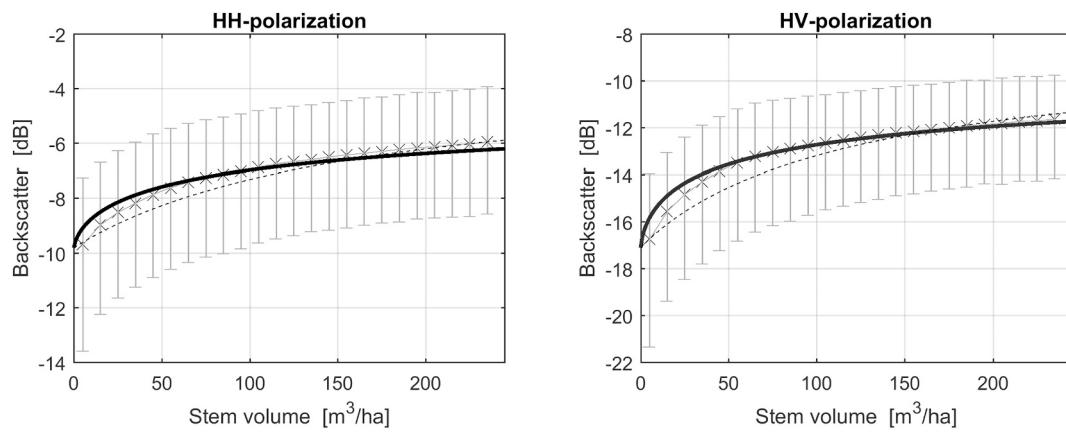


Fig. 11. Modeled backscatter using the WCM in Eq. (6) and in Eq. (9) (solid and dashed curves, respectively) for an ALOS PALSAR image acquired over a 30 km × 30 km tile in northern Sweden on 28 June 2010. The backscatter observations grouped into 10 m³/ha wide intervals of stem volume are illustrated in the form of average values (crosses) and 5th to 95th percentile (vertical bars).

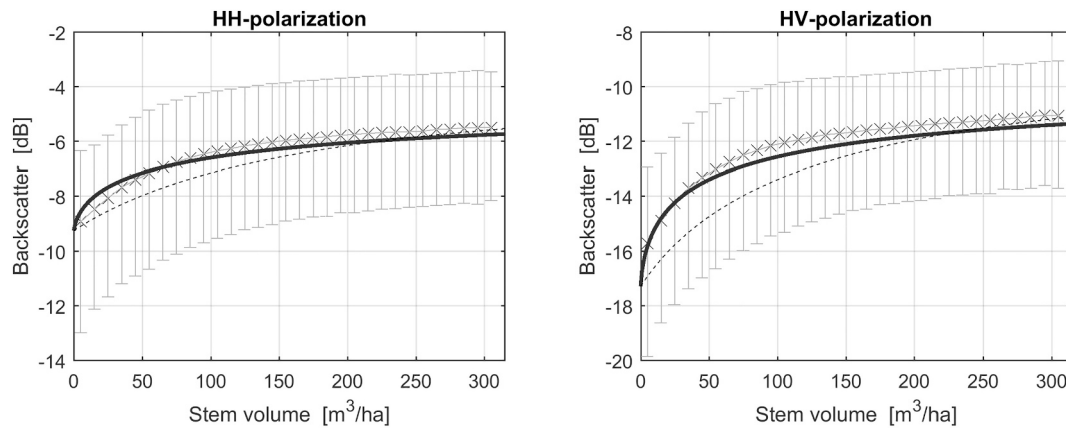


Fig. 12. Modeled backscatter using the WCM in Eq. (6) and in Eq. (9) (solid and dashed curves, respectively) for an ALOS PALSAR image acquired over a 30 km × 30 km tile in southern Sweden on 9 August 2010. The backscatter observations grouped into 10 m³/ha wide intervals of stem volume are illustrated in the form of average values (crosses) and 5th to 95th percentile (vertical bars).

The scatter plot shows the distribution of stem volume estimates in the map for each of 10 m³/ha wide interval of NFI stem volumes. This comparison is, however, little informative on the capability of the retrieval approach to predict stem volume because of the dilution bias occurring when comparing plot-based with pixel-based estimates when the plot size is different than the pixel size (Réjou-Méchain et al., 2014). This effect is due to the strong variability of AGB at small spatial scales and is averaged out when considering multiple samples. Indeed, it is remarked that NFI measurements are part of a sampling strategy aiming at providing information on the statistical distribution of stem volumes for a larger area. Accordingly, retrieval statistics were not computed at plot or pixel level.

The same comparison was undertaken at the level of tile-based averages (Fig. 15). To understand whether the number of plots available in a tile could impact the agreement between the NFI-based and the PALSAR-based pixel averages, the analysis was undertaken separately for tiles containing a small number of plots (symbolized by dots in Fig. 15), an intermediate number of plots (symbolized by crosses in Fig. 15) and the largest number of plots (symbolized by circles in Fig. 15). Interpretation of the results in Fig. 15 was aided by the RMSE relative to the average of the stem volume from the NFI dataset (relative RMSE), the difference between average stem volume from the map and from the NFI dataset (bias) and the coefficient of determination (R^2). The impact of the number of NFI plots on the retrieval statistics is illustrated in Fig. 16, where the relative RMSE, bias and R^2 are displayed

when considering only those tiles that satisfied the requirement of a minimum number of NFI plots. Even for the largest threshold of 20 plots within a tile, the retrieval statistics were based on approximately 200 tiles.

6. Discussion

In this study, we revisited the WCM to estimate stem volume with the objective of explaining, and possibly compensating for, systematic biases occurring with straightforward implementations of the WCM in both low and high biomass forest. Our working assumption was that such biases were a consequence of an oversimplification in the WCM when expressed directly as a function of a biomass-related forest variable, i.e., stem volume or above-ground biomass. Revisiting the WCM implied revisiting the assumption that simple functions could be used to express the forest backscatter as a function of stem volume (Pulliainen et al., 1994; Fransson and Israelsson, 1999; Santoro et al., 2002). Such an investigation was possible thanks to the availability of a spatially dense set of laser observations from the ICESat GLAS instrument from which measurements of two of the predictors in the original version of the WCM (Askne et al., 1997), i.e., canopy cover and canopy height, could be derived.

We identified intriguing trends relating canopy density and a metric of canopy height, closely related to the total vegetation height in the ICESat GLAS observations (Figs. 3 and 4). An exponential model relating

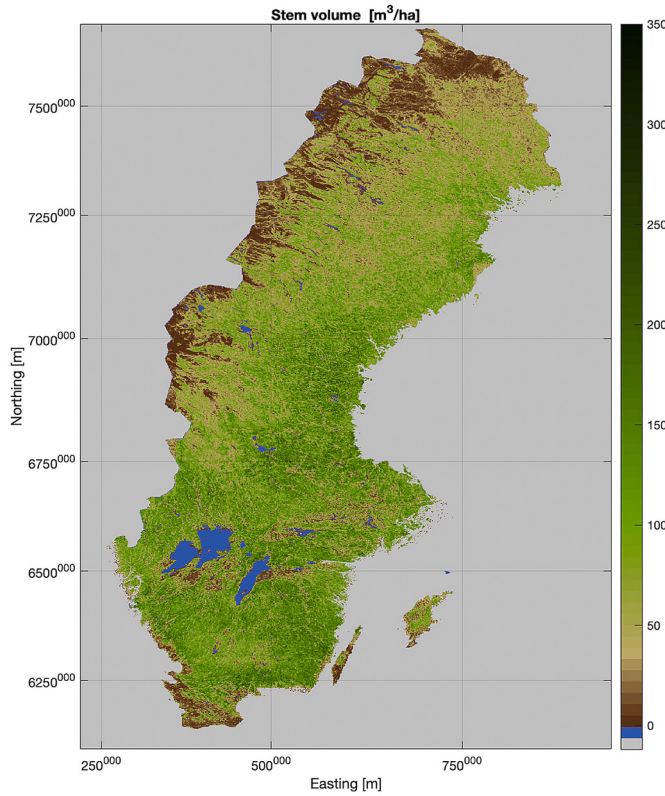


Fig. 13. Stem volume map of Sweden representative for the year 2010 based on repeated dual-polarized observations of the SAR backscatter by ALOS PALSAR.

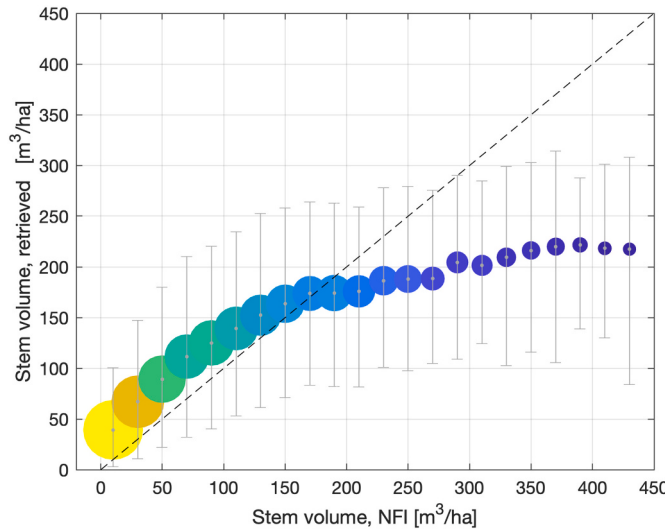


Fig. 14. Scatter plot comparing individual stem volumes from the Swedish NFI and corresponding pixel-based estimates from the ALOS PALSAR dataset. The PALSAR-based estimates were stratified by $10 \text{ m}^3/\text{ha}$ wide stem volume intervals of NFI stem volumes. Each circle represents the average stem volume from the NFI data and the map. The size of the circles and their color are proportional to the number of field inventory plots in a given interval of NFI stem volumes. The vertical bars represent the interquartile range of the map estimates in each interval of stem volumes.

canopy density with canopy height obtained from laser measurements had a highly predictive power (Fig. 3) across Sweden. Our analysis, in addition, indicated that the allometry varied throughout Sweden (Fig. 4), which was interpreted as a consequence of spatial variability of

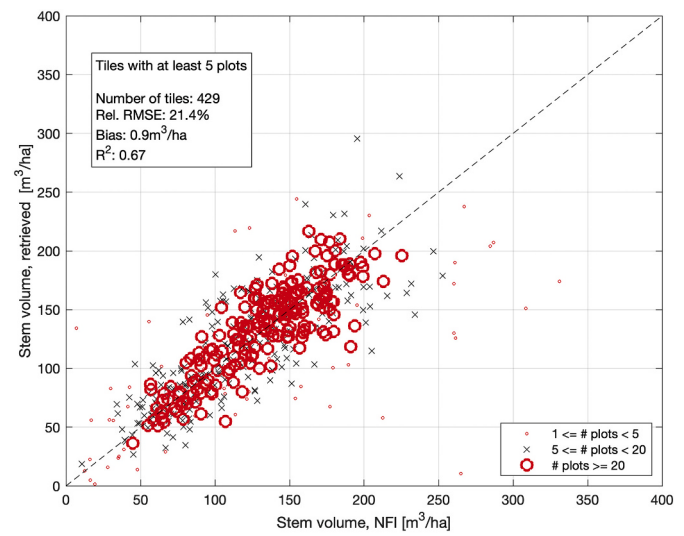


Fig. 15. Scatter plot between NFI stem volume averages and corresponding averages from the estimates based on the ALOS PALSAR dataset at tile level.

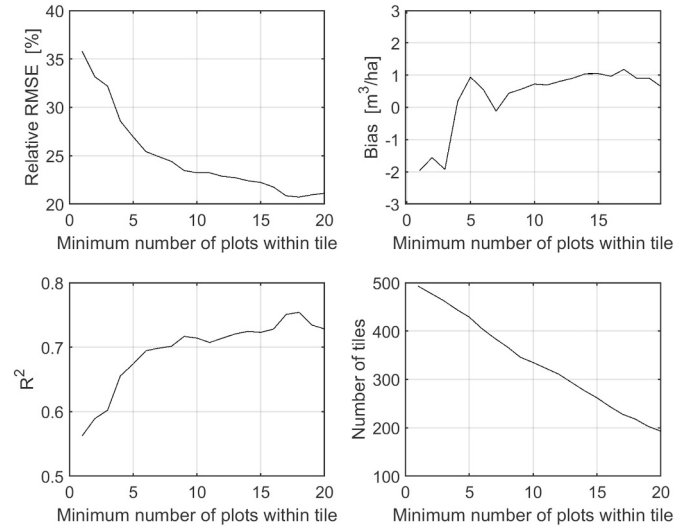


Fig. 16. Retrieval statistics of stem volume at tile level as a function of a minimum number of plots within a tile.

forest composition and structure. Although not shown here, a preliminary investigation has revealed that canopy density and canopy height estimated from ICESat GLAS waveform data are strongly associated in other forest biomes as well and the relationship between the two metrics is explained with the same allometry as in Eq. (2). This aspect is crucial to assess whether the retrieval approach prototyped in this study could be expanded to larger areas.

The validity of an allometry relating forest height and stem volume based on a power-law function was confirmed with NFI data throughout Sweden (Fig. 6). Thanks to the availability of country-wide NFI data, such dependency could be explored at the local scale as well (Fig. 7). At the country scale, the predictive power of this allometry ($R^2 = 0.73$) was higher compared to the allometry relating canopy density and canopy height ($R^2 = 0.42$) (Fig. 6). Differently than in the case of the parameter in Eq. (2) relating canopy density and height, the two parameters of the height-to-stem volume allometry in Eq. (3) varied throughout Sweden (Fig. 7) but did not show any spatial pattern, which we assumed to be related to forest management practices in Sweden. As a result, it was decided to use a single realization of the allometry for the whole

country, a simplification that might have impacted the stem volume estimates locally but not the overall spatial trends.

In this study, we assumed that canopy density and height estimated from the ICESat GLAS waveforms represent measurements for the area-fill factor and the vegetation height in Eq. (6). Also, we used different datasets to characterize the two allometries in Section 4.1, i.e. ICESat GLAS and NFI data. Unfortunately, our database did not include ICESat GLAS footprints in correspondence of the NFI plot locations, which did not allow us to undertake a joint analysis of LiDAR metrics and inventory measurements to confirm the assumption that the two allometries in Eqs. (2, 3) may be combined in order to express canopy density ultimately as a function of stem volume.

A power-law function such as in Eq. (3) was found to describe the relationship between height metrics and AGB from laser scanning data as well (Asner and Mascaro, 2014; Coomes et al., 2017; Labrière et al., 2018) so that in principle the same approach could be extended to estimate forest above-ground biomass provided that measurements of AGB are taken in correspondence of the laser footprints to assess the properties of this allometry. The spatial patterns of the power-law function need to be understood first, though, to avoid biasing biomass estimates when such allometry is used in the retrieval model here proposed.

The ICESat GLAS measurements of canopy density and height were used to constrain the estimate of the tree transmissivity parameter α with Eq. (6). The approach trying to relate observations of the backscatter with the LiDAR metrics to constrain the parameter α returned estimates in agreement with values from previous investigations, i.e. around 0.5 dB/m. Furthermore, we observed a broad geographic pattern although characterized by large scatter (Figs. 8 and 9).

With the ICESat GLAS metrics, it was also possible to simulate two-way forest transmissivity with Eq. (8). These simulations revealed that the forest transmissivity decays rapidly for increasing stem volume in young regrowing forest. After that, the rate of decay decreased for mature forest, remaining almost constant for high biomass forests (Fig. 10). Our results also indicate that the forest transmissivity predicted with a simple exponential function of stem volume did not correspond to the observations (Fig. 10). As a result, the forest backscatter predicted by a WCM combined with allometries was closer to the observations compared to values obtained with the WCM expressed as a direct function of stem volume (Figs. 11 and 12). Although the sensitivity of the L-band backscatter to stem volume was moderate, we report an up to threefold difference between stem volumes estimated with the two versions of the WCM (Figs. 11 and 12).

The stem volume estimates of Sweden obtained from the multi-temporal dataset of ALOS PALSAR observations (Fig. 13) reproduced the gradient of increasing stem volume from North to South and from West to East (Fig. 1c) related to warmer and wetter climate. The plot-to-pixel comparison (Fig. 14) indicated a slight overestimation below 100 m³/ha and underestimation above 200 m³/ha. In addition, only 23% of the variance in the plot measurement was explained by the PALSAR-based values, as also illustrated by the large dispersion of the data points in Fig. 14. The apparently smaller stem volume range obtained with the ALOS PALSAR data compared to the NFI measurements was explained by the dilution bias (Réjou-Méchain et al., 2014) and the different nature of the PALSAR-based and the inventory plot values (Rodríguez-Veiga et al., 2019; Saatchi et al., 2011). Averaging stem volumes measured at plots within a tile and averaging the corresponding estimates from remote sensing data improved the correlation between in situ and retrieved values (Fig. 15). Poor agreement between NFI-based and PALSAR-based averages was found for tiles containing less than five plots, thus being irrelevant for assessing the performance of the retrieval (Fig. 15).

The retrieval statistics in Fig. 15 indicate unbiased estimates and a relative RMSE of 21.4% at the aggregated level of the tiles. It is here remarked that each data point in Fig. 15 represents the mean value over a certain number of NFI plots within the tile and the corresponding pixels covered by the area of each plot. Hence, the scatter plot in Fig. 15

must be interpreted as validation at hectare scale similar to a validation undertaken when comparing averages at forest stand level. The importance of evaluating the retrieval at aggregated level is further illustrated in Fig. 16. The relative RMSE, the estimation bias and the coefficient of determination decreased when excluding from the evaluation tiles containing a number of inventory plots below a given threshold. Even for the largest threshold of 20 plots within a tile, the retrieval statistics were based on approximately 200 tiles. While the relative RMSE decreased to about 20–25% of the mean stem volume and the coefficient of determination increased to about 0.75 for increasing number of plots within a tile, the bias remained constant close to the 0 m³/ha level. These results are indicative with respect to the number of sample plots to be used when assessing the accuracy of maps based on remote sensing images.

7. Conclusion

Our work combined the WCM with allometric equations to provide a fully parametric retrieval model for forest biomass (here represented by the forest variable as stem volume) using L-band SAR backscatter measurements as predictors. Complementing the WCM with allometries improved the fit to the observations compared to simpler expressions of the WCM. Thanks to the combination of individual estimates of stem volume from multiple observations of the backscatter by ALOS PALSAR, the retrieval statistics indicate unbiased estimates for averages based on at least five pixels, i.e., an area larger than 0.3 ha. Having demonstrated here the potential of combining allometries and retrieval models based on microwave observations, future studies shall expand to confirm whether this approach is suitable in other forested environments. For cases requiring an estimate of AGB instead of stem volume, an additional step to characterize the relationship between stem volume and AGB or canopy height and AGB would be necessary. A forest biomass (stem volume or AGB) retrieval scheme that performs across forest types and can be considered as candidate of wall-to-wall forest biomass retrieval is of great importance in the context of forest biomass estimation from short-wavelength SAR backscatter observations. Our results confirm the suitability of a dataset of multiple L-band backscatter observations to estimate stem volume, i.e. a biomass-related variable, in boreal forest. Finally, we consider the results of this study of utmost importance for the planning of observations by future L-band satellite missions with a target of forest observations (ALOS-4, NiSAR and ROSE-L).

Declaration of Competing Interest

None.

Acknowledgments

We are thankful to Prof. Jan Askne and the three anonymous Reviewers for constructive criticisms and suggestions to improve the manuscript. This work was financially supported by the Swedish National Space Agency and was undertaken within the framework of the JAXA Kyoto & Carbon Initiative. ALOS PALSAR data have been provided by JAXA EORC. We acknowledge the Swedish National Land Survey (Lantmäteriet) for providing the DEMs used in the SAR image geocoding. In this study, we used version 5 of the MODIS VCF dataset; the most recent version (V6) is currently available at <https://lpdaac.usgs.gov/products/mod44bv006/>.

References

- Alekseev, A., Tomppo, E., McRoberts, R.E., von Gadow, K., 2019. A constructive review of the state Forest inventory in the Russian Federation. *For. Ecosyst.* 6, 9. <https://doi.org/10.1186/s40663-019-0165-3>.
- Antropov, O., Rauste, Y., Ahola, H., Häme, T., 2013. Stand-level stem volume of boreal forests from spaceborne SAR imagery at L-band. *IEEE J. Sel. Top. Earth Observ. Remote Sens.* 6, 35–44. <https://doi.org/10.1109/JSTARS.2013.2241018>.

- Askne, J., Santoro, M., 2012. Experiences in boreal forest stem volume estimation from multitemporal C-band InSAR. In: Padron, I. (Ed.), Recent Interferometry Applications in Topography and Astronomy. InTech. <https://doi.org/10.5772/35102>.
- Askne, J., Dampert, P.B.G., Ulander, L.M.H., Smith, G., 1997. C-band repeat-pass interferometric SAR observations of the forest. *IEEE Trans. Geosci. Remote Sens.* 35, 25–35.
- Askne, J., Fransson, J., Santoro, M., Soja, M., Ulander, L., 2013. Model-based biomass estimation of a hemi-boreal forest from multitemporal TanDEM-X acquisitions. *Remote Sens.* 5, 5574–5597. <https://doi.org/10.3390/rs5115574>.
- Askne, J.I.H., Santoro, M., 2015. On the estimation of boreal forest biomass from TanDEM-X data without training samples. *IEEE Geosci. Remote Sensing Lett.* 12, 771–775. <https://doi.org/10.1109/LGRS.2014.2361393>.
- Asner, G.P., Mascaro, J., 2014. Mapping tropical forest carbon: calibrating plot estimates to a simple LiDAR metric. *Remote Sens. Environ.* 140, 614–624. <https://doi.org/10.1016/j.rse.2013.09.023>.
- Attema, E.P.W., Ulaby, F.T., 1978. Vegetation modeled as a water cloud. *Radio Sci.* 13, 357–364.
- Bar-On, Y.M., Phillips, R., Milo, R., 2018. The biomass distribution on earth. *Proc. Natl. Acad. Sci. U. S. A.* 115, 6506–6511. <https://doi.org/10.1073/pnas.1711842115>.
- Bouvet, A., Mermoz, S., Le Toan, T., Villard, L., Mathieu, R., Naidoo, L., Asner, G.P., 2018. An above-ground biomass map of African savannahs and woodlands at 25 m resolution derived from ALOS PALSAR. *Remote Sens. Environ.* 206, 156–173. <https://doi.org/10.1016/j.rse.2017.12.030>.
- Carreiras, J.M.B., Vasconcelos, M.J., Lucas, R.M., 2012. Understanding the relationship between aboveground biomass and ALOS PALSAR data in the forests of Guinea-Bissau (West Africa). *Remote Sens. Environ.* 121, 426–442. <https://doi.org/10.1016/j.rse.2012.02.012>.
- Carreiras, J.M.B., Melo, J.B., Vasconcelos, M.J., 2013. Estimating the above-ground biomass in miombo savanna woodlands (Mozambique, East Africa) using L-band synthetic aperture radar data. *Remote Sens.* 5, 1524–1548. <https://doi.org/10.3390/rs5041524>.
- Cartus, O., Kellndorfer, J., Rombach, M., Walker, W., 2012a. Mapping canopy height and growing stock volume using airborne lidar, alos palsar and landsat ETM+. *Remote Sens.* 4, 3320–3345. <https://doi.org/10.3390/rs4113320>.
- Cartus, O., Santoro, M., Kellndorfer, J., 2012b. Mapping forest aboveground biomass in the northeastern United States with ALOS PALSAR dual-polarization L-band. *Remote Sens. Environ.* 124, 466–478. <https://doi.org/10.1016/j.rse.2012.05.029>.
- Cartus, O., Kellndorfer, J., Walker, W., Franco, C., Bishop, J., Santos, L., Fuentes, J.M.M., 2014. A national, detailed map of forest aboveground carbon stocks in Mexico. *Remote Sens.* 6, 5559–5588. <https://doi.org/10.3390/rs6065559>.
- Cartus, Santoro, Wegmüller, Rommen, 2019. Benchmarking the retrieval of biomass in boreal forests using P-band SAR backscatter with multi-temporal C- and L-band observations. *Remote Sens.* 11, 1695. <https://doi.org/10.3390/rs11141695>.
- Ciais, P., Dolman, A.J., Bombelli, A., Duren, R., Peregon, A., Rayner, P.J., Miller, C., Gobron, N., Kinderman, G., Marland, G., Gruber, N., Chevallier, F., Andres, R.J., Balsamo, G., Bopp, L., Bréon, F.-M., Broquet, G., Dargaville, R., Battin, T.J., Borges, A., Bovensmann, H., Buchwitz, M., Butler, J., Canadell, J.G., Cook, R.B., DeFries, R., Engelen, R., Gurney, K.R., Heineke, C., Heimann, M., Held, A., Henry, M., Law, B., Luyssaert, S., Miller, J., Moriyama, T., Moulin, C., Myreni, R.B., Nussli, C., Obersteiner, M., Ojima, D., Pan, Y., Paris, J.-D., Piao, S.L., Poultier, B., Plummer, S., Quegan, S., Raymond, P., Reichstein, M., Rivier, L., Sabine, C., Schimel, D., Tarasova, O., Valentini, R., Wang, R., van der Werf, G., Wickland, D., Williams, M., Zehner, C., 2014. Current systematic carbon-cycle observations and the need for implementing a policy-relevant carbon observing system. *Biogeosciences* 11, 3547–3602. <https://doi.org/10.5194/bg-11-3547-2014>.
- Coomes, D.A., Dalponte, M., Jucker, T., Asner, G.P., Banin, L.F., Burslem, D.F.R.P., Lewis, S.L., Nilus, R., Phillips, O.L., Phua, M.-H., Qie, L., 2017. Area-based vs tree-centric approaches to mapping forest carbon in southeast Asian forests from airborne laser scanning data. *Remote Sens. Environ.* 194, 77–88. <https://doi.org/10.1016/j.rse.2017.03.017>.
- Dobson, M.C., Ulaby, F.T., LeToan, T., Beaudoin, A., Kasischke, E.S., Christensen, N., 1992. Dependence of radar backscatter on coniferous forest biomass. *IEEE Trans. Geosci. Remote Sens.* 30, 412–415. <https://doi.org/10.1109/36.134090>.
- Fransson, J.E.S., Israelsson, H., 1999. Estimation of stem volume in boreal forests using ERS-1 C- and JERS-1 L-band SAR data. *Int. J. Remote Sens.* 20, 123–137. <https://doi.org/10.1080/014311699213640>.
- Gillis, M.D., Omule, A.Y., Brierley, T., 2005. Monitoring Canada's forests: the National Forest Inventory. *For. Chron.* 81, 214–221. <https://doi.org/10.5558/tfc81214-2>.
- Hansen, M.C., DeFries, R.S., Townshend, J.R.G., Carroll, M., Dimiceli, C., Sohlberg, R.A., 2003. Global percent tree cover at a spatial resolution of 500 meters: first results of the MODIS vegetation continuous fields algorithm. *Earth Interact.* 7, 1–15. [https://doi.org/10.1175/1087-3562\(2003\)007<0001:GPTCAA>2.0.CO;2](https://doi.org/10.1175/1087-3562(2003)007<0001:GPTCAA>2.0.CO;2).
- Hansen, M.C., Potapov, P.V., Moore, R., Hansen, M., Turubanova, S.A., Tyukavina, A., Thau, D., Stehman, S.V., Goetz, S.J., Loveland, T.R., Komiareddy, A., Egorov, A., Chini, L., Justice, C.O., Townshend, J.R.G., 2013. High-resolution global maps of 21st century forest cover change. *Science* 342, 850–853.
- Harrell, P.A., Bourgeau-Chavez, L.L., Kasischke, E.S., French, N.H.F., Christensen Jr., N. L., 1995. Sensitivity of ERS-1 and JERS-1 radar data to biomass and stand structure in Alaskan boreal forest. *Remote Sens. Environ.* 54, 247–260.
- Hilbert, C., Schmullius, C., 2012. Influence of surface topography on ICESat/GLAS forest height estimation and waveform shape. *Remote Sens.* 4, 2210–2235. <https://doi.org/10.3390/rs4082210>.
- Imhoff, M.L., 1995. Radar backscatter and biomass saturation: ramifications for global biomass inventory. *IEEE Trans. Geosci. Remote Sens.* 33, 511–518.
- Jenkins, J.C., Chojnacky, D.C., Heath, L.S., Birdsey, R.A., 2003. National-scale biomass estimators for United States tree species. *For. Sci.* 49, 12–35.
- Kasischke, E.S., Bourgeau-Chavez, L.L., Christensen Jr., N.L., Haney, E., 1994. Observations on the sensitivity of ERS-1 SAR image intensity to changes in aboveground biomass in young loblolly pine forests. *Int. J. Remote Sens.* 15, 3–16.
- Koch, B., 2010. Status and future of laser scanning, synthetic aperture radar and hyperspectral remote sensing data for forest biomass assessment. *ISPRS J. Photogramm. Remote Sens.* 65, 581–590. <https://doi.org/10.1016/j.isprsjprs.2010.09.001>.
- Kurvenen, L., Pulliainen, J., Hallikainen, M., 1999. Retrieval of biomass in boreal forests from multitemporal ERS-1 and JERS-1 SAR images. *IEEE Trans. Geosci. Remote Sens.* 37, 198–205.
- Labrière, N., Tao, S., Chave, J., Scipal, K., Toan, T.L., Abernethy, K., Alonso, A., Barbier, N., Bissengou, P., Casal, T., Davies, S.J., Ferraz, A., Herault, B., Jaouen, G., Jeffery, K.J., Kenfack, D., Korte, L., Lewis, S.L., Malhi, Y., Memigah, H.R., Poulsen, J.R., Rejou-Méchain, M., Villard, L., Vincent, G., White, L.J.T., Saatchi, S., 2018. In situ reference datasets from the TropiSAR and AfriSAR campaigns in support of upcoming Spaceborne biomass missions. *IEEE J. Sel. Top. Appl. Earth Observ. Remote Sens.* 11, 3617–3627. <https://doi.org/10.1109/JSTARS.2018.2851606>.
- Lantmäteriet, 2010. *Produktbeskrivning: GSD-Höjdata - grid 50+ hdb*.
- Lantmäteriet, 2019. Quality Description of National Elevation Model, 2019, 20 August 2019, version 1.4 (last accessed on 3 September 2020). https://www.lantmateriet.se/globalassets/kartor-och-geografisk-information/hojdata/quality_description_grid.pdf.
- Los, S.O., Rosette, J.A.B., Kljun, N., North, P.R.J., Chasmer, L., Suárez, J.C., Hopkinson, C., Hill, R.A., Van Gorsel, E., Mahoney, C., Berni, J.A.J., 2012. Vegetation height and cover fraction between 60° S and 60° N from ICESat GLAS data. *Geosci. Model Dev.* 5, 413–432. <https://doi.org/10.5194/gmd-5-413-2012>.
- Lu, D., Chen, Q., Wang, G., Liu, L., Li, G., Moran, E., 2016. A survey of remote sensing-based aboveground biomass estimation methods in forest ecosystems. *Intern. J. Dig. Earth* 9, 63–105. <https://doi.org/10.1080/17538947.2014.990526>.
- Luckman, A., Baker, J., Kuplich, T.M., da Costa Freitas Yanasse, C., Frery, A.C., 1997. A study of the relationship between radar backscatter and regenerating tropical forest biomass for spaceborne SAR instruments. *Remote Sens. Environ.* 60, 1–13.
- Mermoz, S., Le Toan, T., Villard, L., Réjou-Méchain, M., Seifert-Granzin, J., 2014. Biomass assessment in the Cameroonian savanna using ALOS PALSAR data. *Remote Sens. Environ.* 155, 109–119. <https://doi.org/10.1016/j.rse.2014.01.029>.
- Michelakis, D., Stuart, N., Brolly, M., Woodhouse, I.H., Lopez, G., Linares, V., 2015. Estimation of woody biomass of pine savanna woodlands from ALOS PALSAR images. *IEEE J. Sel. Top. Appl. Earth Observ. Remote Sens.* 8, 244–254.
- Mitchard, E.T.A., Saatchi, S.S., Woodhouse, I.H., Nangendo, G., Ribeiro, N.S., Williams, M., Ryan, C.M., Lewis, S.L., Feldpausch, T.R., Meir, P., 2009. Using satellite radar backscatter to predict above-ground woody biomass: a consistent relationship across four different African landscapes. *Geophys. Res. Lett.* 36, 1–6. <https://doi.org/10.1029/2009GL040692>.
- Mitchard, E.T.A., Saatchi, S.S., White, L.J.T., Abernethy, K.A., Jeffery, K.J., Lewis, S.L., Collins, M., Lefsky, M.A., Leal, M.E., Woodhouse, I.H., Meir, P., 2012. Mapping tropical forest biomass with radar and spaceborne LiDAR in Lopé National Park, Gabon: overcoming problems of high biomass and persistent cloud. *Biogeosciences* 9, 179–191. <https://doi.org/10.5194/bg-9-179-2012>.
- Nilsson, M., Nordkvist, K., Jonzén, J., Lindgren, N., Axensten, P., Wallerman, J., Egberth, M., Larsson, S., Nilsson, L., Eriksson, J., Olsson, H., 2017. A nationwide forest attribute map of Sweden predicted using airborne laser scanning data and field data from the national forest inventory. *Remote Sens. Environ.* 194, 447–454. <https://doi.org/10.1016/j.rse.2016.10.022>.
- Pulliainen, J.T., Heiska, K., Hyypä, J., Hallikainen, M.T., 1994. Backscattering properties of boreal forests at the C- and X-bands. *IEEE Trans. Geosci. Remote Sens.* 32, 1041–1050.
- Pulliainen, J.T., Kurvenen, L., Hallikainen, M.T., 1999. Multitemporal behavior of L- and C-band SAR observations of boreal forests. *IEEE Trans. Geosci. Remote Sens.* 37, 927–937.
- Ranson, K.J., Saatchi, S.S., Sun, G., 1995. Boreal forest ecosystem characterization with SIR-C/XSAR. *IEEE Trans. Geosci. Remote Sens.* 33, 867–876.
- Ranson, K.J., Sun, G., Lang, R.H., Chauhan, N.S., Cacciola, R.J., Kilic, O., 1997. Mapping of boreal forest biomass from spaceborne synthetic aperture radar. *J. Geophys. Res.* 102, 29599–29610.
- Réjou-Méchain, M., Muller-Landau, H.C., Dettò, M., Thomas, S.C., Le Toan, T., Saatchi, S.S., Barreto-Silva, J.S., Bourg, N.A., Bunyavejchewin, S., Butt, N., Brockelman, W.Y., Cao, M., Cárdenas, D., Chiang, J.-M., Chuyong, G.B., Clay, K., Condit, R., Dattaraja, H.S., Davies, S.J., Duque, A., Esufali, S., Ewangbo, C., Fernando, R.H.S., Fletcher, C.D., Gunatileke, I.A.U.N., Hao, Z., Harms, K.E., Hart, T.B., Hérault, B., Howe, R.W., Hubbell, S.P., Johnson, D.J., Kenfack, D., Larson, A.J., Lin, L., Lin, Y., Lutz, J.A., Makana, J.-R., Malhi, Y., Marthews, T.R., McEwan, R.W., McMahon, S.M., McShea, W.J., Muscarella, R., Nathangal, A., Noor, N.S.M., Nyctch, C.J., Oliveira, A.A., Phillips, R.P., Pongattanaranuk, N., Punchi-Manage, R., Salim, R., Schurman, J., Sukumar, R., Suresh, H.S., Suwanvecho, U., Thomas, D.W., Thompson, J., Urface, M., Valencia, R., Vicentini, A., Wolf, A.T., Yap, S., Yuan, Z., Zartman, C.E., Zimmerman, J.K., Chave, J., 2014. Local spatial structure of forest biomass and its consequences for remote sensing of carbon stocks. *Biogeosciences* 11, 6827–6840. <https://doi.org/10.5194/bg-11-6827-2014>.
- Rodríguez-Veiga, P., Quegan, S., Carreiras, J., Persson, H.J., Fransson, J.E.S., Hoscilo, A., Ziolkowski, D., Stereńczak, K., Lohberger, S., Stängel, M., Berninger, A., Siegert, F., Avitabile, V., Herold, M., Mermoz, S., Bouvet, A., Le Toan, T., Carvalhalis, N., Santoro, M., Cartus, O., Rauste, Y., Mathieu, R., Asner, G.P., Thiel, C., Pathe, C., Schmullius, C., Seifert, F.M., Tansey, K., Balzter, H., 2019. Forest biomass retrieval

- approaches from earth observation in different biomes. *Int. J. Appl. Earth Obs. Geoinf.* 77, 53–68. <https://doi.org/10.1016/j.jag.2018.12.008>.
- Rosenqvist, A., Shimada, M., Suzuki, S., Ohgushi, F., Tadono, T., Watanabe, M., Tsuzuku, K., Watanabe, T., Kamijo, S., Aoki, E., 2014. Operational performance of the ALOS global systematic acquisition strategy and observation plans for ALOS-2 PALSAR-2. *Remote Sens. Environ.* 155, 3–12. <https://doi.org/10.1016/j.rse.2014.04.011>.
- Ryan, C.M., Hill, T., Woollen, E., Ghee, C., Mitchard, E., Cassells, G., Grace, J., Woodhouse, I.H., Williams, M., 2012. Quantifying small-scale deforestation and forest degradation in African woodlands using radar imagery. *Glob. Chang. Biol.* 18, 243–257. <https://doi.org/10.1111/j.1365-2486.2011.02551.x>.
- Saatchi, S., Marlier, M., Chazdon, R.L., Clark, D.B., Russell, A.E., 2011. Impact of spatial variability of tropical forest structure on radar estimation of aboveground biomass. *Remote Sens. Environ.* 115, 2836–2849. <https://doi.org/10.1016/j.rse.2010.07.015>.
- Santoro, M., Cartus, O., 2018. Research pathways of Forest above-ground biomass estimation based on SAR backscatter and Interferometric SAR observations. *Remote Sens.* 10, 608. <https://doi.org/10.3390/rs10040608>.
- Santoro, M., Askne, J., Smith, G., Fransson, J.E.S., 2002. Stem volume retrieval in boreal forests from ERS-1/2 interferometry. *Remote Sens. Environ.* 81, 19–35.
- Santoro, M., Eriksson, L., Askne, J., Schmullius, C., 2006. Assessment of stand-wise stem volume retrieval in boreal forest from JERS-1 L-band SAR backscatter. *Int. J. Remote Sens.* 27, 3425–3454.
- Santoro, M., Shvidenko, A., McCallum, I., Askne, J., Schmullius, C., 2007. Properties of ERS-1/2 coherence in the Siberian boreal forest and implications for stem volume retrieval. *Remote Sens. Environ.* 106, 154–172. <https://doi.org/10.1016/j.rse.2006.08.004>.
- Santoro, M., Beer, C., Cartus, O., Schmullius, C., Shvidenko, A., McCallum, I., Wegmüller, U., Wiesmann, A., 2011. Retrieval of growing stock volume in boreal forest using hyper-temporal series of Envisat ASAR ScanSAR backscatter measurements. *Remote Sens. Environ.* 115, 490–507. <https://doi.org/10.1016/j.rse.2010.09.018>.
- Santoro, M., Eriksson, L.E.B., Fransson, J.E.S., 2015. Reviewing ALOS PALSAR backscatter observations for stem volume retrieval in Swedish forest. *Remote Sens.* 7, 4290–4317.
- Santoro, M., Cartus, O., Fransson, J.E.S., Wegmüller, U., 2019. Complementarity of X-, C-, and L-band SAR backscatter observations to retrieve Forest stem volume in boreal Forest. *Remote Sens.* 11, 1563. <https://doi.org/10.3390/rs11131563>.
- Sarker, M.L.R., Nichol, J., Ahmad, B., Busu, I., Rahman, A.A., 2012. Potential of texture measurements of two-date dual polarization PALSAR data for the improvement of forest biomass estimation. *ISPRS J. Photogramm. Remote Sens.* 69, 146–166. <https://doi.org/10.1016/j.isprsjprs.2012.03.002>.
- Sexton, J.O., Song, X.P., Feng, M., Noojipady, P., Anand, A., Huang, C., Kim, D.H., Collins, K.M., Channan, S., DiMiceli, C., Townshend, J.R., 2013. Global, 30-m resolution continuous fields of tree cover: Landsat-based rescaling of MODIS vegetation continuous fields with lidar-based estimates of error. *Intern. J. Dig. Earth* 6, 427–448. <https://doi.org/10.1080/17538947.2013.786146>.
- Shimada, M., Isoguchi, O., Tadono, T., Isono, K., 2009. PALSAR radiometric and geometric calibration. *IEEE Trans. Geosci. Remote Sens.* 47, 3915–3932.
- Simard, M., Pinto, N., Fisher, J.B., Baccini, A., 2011. Mapping forest canopy height globally with spaceborne lidar. *J. Geophys. Res.* 116 <https://doi.org/10.1029/2011JG001708>.
- Sun, G., Ranson, K.J., Guo, Z., Zhang, Z., Montesano, P., Kimes, D., 2011. Forest biomass mapping from lidar and radar synergies. *Remote Sens. Environ.* 115, 2906–2916. <https://doi.org/10.1016/j.rse.2011.03.021>.
- Thapa, R.B., Motohka, T., Watanabe, M., Shimada, M., 2015. Time-series maps of aboveground carbon stocks in the forests of Central Sumatra. *Carbon Bal. Manage.* 10 <https://doi.org/10.1186/s13021-015-0034-5>.
- Tomppo, E., Gschwantner, T., Lawrence, M., McRoberts, R.E., 2010. National Forest Inventories - Pathways for Common Reporting. Springer Science and Business Media.
- Ulander, L.M.H., 1996. Radiometric slope correction of synthetic-aperture radar images. *IEEE Trans. Geosci. Remote Sens.* 34, 1115–1122.
- Wegmüller, U., 1999. In: IGARSS'99 (Ed.), Automated Terrain Corrected SAR Geocoding. IEEE Publications, Piscataway, NJ, pp. 1712–1714.
- Wegmüller, U., Werner, C., Strozzi, T., Wiesmann, A., 2002. Automated and precise image registration procedures. In: Bruzzone, Smits (Ed.), Analysis of Multi-Temporal Remote Sensing Images, Series in Remote Sensing. World Scientific, Trento, pp. 37–49, 13–14 September 2001.
- Yu, Y., Saatchi, S., 2016. Sensitivity of L-band SAR backscatter to aboveground biomass of global forests. *Remote Sens.* 8 <https://doi.org/10.3390/rs8060522>.
- Zianis, D., Mencuccini, M., 2004. On simplifying allometric analyses of forest biomass. *For. Ecol. Manag.* 187, 311–332. <https://doi.org/10.1016/j.foreco.2003.07.007>.